# Modelling of the Effect of Discontinuities on the Extent of the Fracture Zone Surrounding Deep Tunnels

**E. J. Sellers and P. Klerck**

*Abstract —A series of physical and numerical model tests were performed to investigate the behaviour of the rock surrounding circular excavations under high confining pressures. The aim was to provide information on the formation of fractures around deep level mine tunnels under controlled conditions. Solid cubes containing a circular hole were confined to a vertical pressure of 200 MPa with a confinement of 100 MPa in the two horizontal directions. To provide a contrast, a block was made from a series of plates to simulate the presence of horizontal bedding planes. The resulting fracture patterns are completely different and emphasized that the amount of fracturing would be considerably increased as a result of discontinuities in the rock. Analysis of acoustic emission data provides insights into the response of the rock during loading and unloading, and assists with the identification of the effect of the discontinuities. A model based on Mohr Coulomb plasticity and rotating smeared-crack concepts has been developed to represent the formation of discrete fracture processes in a continuum under compressive and tensile stress conditions. The model is implemented in a discrete element - finite element method and is able to represent the change in fracture patterns between the solid and jointed blocks. This provides confidence for the application of the numerical model to the design of mine tunnels at great depth.* 

## 1 Introduction

More than 500 km of tunnels are excavated annually at depths to 3500 m in South African gold mines. Mining has occurred at increasing depths, and recent initiatives are investigating the possibilities of mining at depths of between 4000 m and 5000 m. There is considerable experience in the development of tunnels at current depths, but it is important to understand whether there will be significant changes in the rock mass response at even greater depths. The questions to be addressed are how the rock fabric and included discontinuities affect the stresses at which the failure initiates, the subsequent failure processes and the support requirements.

The failure of the sidewalls of excavations in rock has been an area of extensive research in rock mechanics as it affects the major problems of borehole breakout in the oil industry (Haimson 1998) and the stability of tunnel sidewalls (Brady and Brown 1993). Most borehole breakout studies are conducted under uniaxial or biaxial loading (Carter 1992 and 1991; Martin 1997, CSIR 1973). A summary of a number of test programs and their relevance to underground tunneling has been produced by Martin (1997).

In uniaxial tests, primary tension fractures initiate at the top and bottom of the hole and extend in the direction of the applied stress. Increased uniaxial stress induces remote fractures that tend to form an approximate diamond shape around the excavation. Finally, slabbing fractures appear on the sides of the hole where the compression is greatest and extend parallel to the sidewalls, causing the characteristic triangular-shaped breakout zone. Experiments in sandstone and granite indicate that the breakout shape may be altered by the applied stress path, the strain rate, the boundary conditions and the excavation shape. (Ewy and Cook 1990a, 1990b; Gay 1973; Barla 1972).

Increasing the confinement prevents the initiation of the primary tension fracture and failure is due to the remote and slabbing fractures (Carter 1992; Ewy and Cook 1990a, 1990b). The lengths of the remote crack decrease with increasing k-ratio (Carter 1991). The effect of the high confining pressures of up to 140 MPa anticipated at depths of up to 5000 m has not been studied in as much detail as for uniaxial loading. Cylindrical specimens of sandstone containing cylindrical holes tested under increasing hydrostatic pressures, up to 275 MPa, indicate that the extent of the fracture zone size increases with increasing pressure, until the entire sample fails (Gay 1973).

Present address: Ewan Sellers, Project Manager, CSIR Miningtek, P.O. Box 91230, Auckland Park, 2006, South Africa (email: esellers@csir.co.za); Paul Klerck, Postgraduate Student, Department of Civil Engineering, University of Wales, Swansea, U.K. SA2 8PP (email: P.A.Klerck@swansea.ac.uk)

This paper was originally published in *Tunnels under Pressure*, the proceedings of the AITES-ITA 2000 World Tunnel Congress. The paper is published herein with the permission of the South African Institute of Mining and Metallurgy and the authors.

www.elsevier.com/locate/tust

*Tunnelling and Underground Space Technology*, Vol. 15, No. 4, pp. 463–469, 2000
0886-7798/00/ $ - see front matter © 2001 South African Institute of Mining and Metallurgy. Published by Elsevier Science Ltd. All rights reserved.
PII: S0886-7798(01)00015-3

Pergamon

Underground experience indicates that the breakout zone will increase in size if the slabbed material is removed by fall-out or by manual scraping, but will stabilize for a given stress state (Martin 1997). Similarly the zone of breakout in deep gold mine ore-passes is extended by the passage of the flow of the rock down the pass (Rech et al. 1992) The breakout zone in boreholes for oil productions may be extended by the action of the fluids (Haimsom 1998).

The extent of the fracture zone surrounding deep level excavations can be considerably increased by the presence of partings planes (Malan and Basson 1998). Rock is an inherently variable material and can contain many different forms of discontinuities. At small scales, these include the pores and crystal structure contained within the grains. On a larger scale, discontinuities are due to the boundaries of the grains, and larger features such as joints, extension veins and faults. Movement on these pre-existing structures alters the state of stress and can induce fracture patterns that are different from the classical borehole breakout.

In small-scale experiments, the shape and extent of the failure zone around holes in Berea sandstone have been found to be influenced by the bedding (Ewy and Cook 1990a). Other experiments with explicit parting planes (Goodman 1972) and observations of the fracture zone surrounding tunnels in gold mines (Roberts et al. 1999; Graham; Bosman et al. 2000) indicate that the partings induce additional fracturing that differs from the classical breakout pattern, being captured within the layers that intersect the tunnel.

Analytical solutions show that the rock friction angle must be less than 19.6° to initiate slip on a discontinuity at 45° to the tunnel side wall (Brady and Brown 1993). However, the inclusion of an elastic stiffness on the bedding induces new tensile regions that would be the site of additional fracturing (Kulhawy1975; Goodman 1972; Barla 1972). The extent of the zones is controlled by the ratio of the shear to normal stiffness specified on the joint.

Many constitutive models for representing rock masses containing multiple joints as an equivalent continuum have been proposed using, for example, the concepts of damage mechanics (Sellers and Scheele 1996, Swoboda 1998) or multilaminate plasticity (Chen and Egger 1999). However, when considering the support requirements and the dynamic response of the extensive fracture zones around deep excavations, it is necessary to be able to represent the large deformations, the stress transfer due to fracture formation during load changes, and the interactions of multiple moving blocks.

A new constitutive model for rock fracture, based on Mohr Coulomb plasticity, is currently being developed. Experiments that were performed on two different sample configurations to provide additional understanding of the mechanisms of rock fractures around openings are used to test the ability of the model to predict the formation of fractures in compressive and tensile stress states.

## 2. Laboratory Tests

### *2.1 Test set-up*

The intention of the project was to apply realistic confinements of up to 200 MPa to large-scale specimens (300-mm cubes); however, the only feasible solution to apply such confinements within the project time frame was to test smaller samples. An existing confining ring for 300-mm samples was modified to permit the inclusion of a high pressure confining system as shown in Figure 1.

The samples are cubes of side length 100 mm. The most difficult part of sample preparation is ensuring that the sides are machined perpendicular to within 0.01°. A 25-mm-diameter hole is diamond-core-drilled halfway through the block. The sample is confined by platens that are

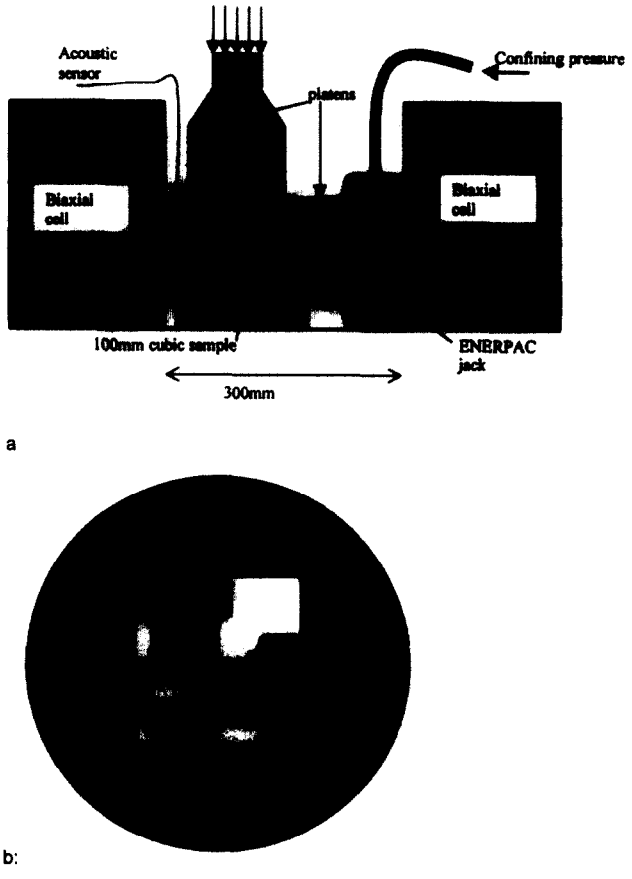


*Figure 1. Schematic of high pressure testing system. a: section b: plan.*

slightly smaller than the sample. This would be unsuitable for a true triaxial test on a solid block, but is satisfactory for these tests with the hole acting as a stress concentrator. Stearic acid was applied to the sides of the samples to minimize friction.

The confining stress is applied by two Enerpack jacks that are rated for 150 tons maximum load. Both jacks are connected to the same hydraulic pump. The maximum gauge pressure on the load pistons of 69 MPa corresponds to a sample stress of 150 MPa. The confinement is applied by manual pumping. The pressure is kept at a given ratio to the vertical applied pressure (k-ratio). The vertical load is applied with a 25-MN loading frame. Loading is applied under stress control at a variable rate. For some of the tests, a piezoelectric acoustic emission (AE) sensor was placed on one of the side platens, and the acoustic emissions were logged simultaneously with the applied load. The AE events are recorded on an MISTRAS system using 1-MHz piezoelectric sensors (PAC S9225). The AE system operates at a data acquisition rate of 4 MHz per channel.

Ten cube tests were performed at high pressure. Four cubes were made from Norite, and the other six were Elsburg Quartzite. The uniaxial compressive strength of the Norite is 125 MPa and that of the Elsburg quartzite is 120MPa. Only the Elsburg Quartzite will be used for comparison with the numerical models in this paper.

Samples were unloaded at various stress states to determine the evolution of the fracture pattern. In order to investigate the effect of a number of parallel discontinuities on the fracture pattern, a sample was prepared, consisting of six plates of 7-mm thick sandwiched between two thicker plates. Experience showed that 7 mm was the thinnest plate that could be cut and ground. The thicker plates at the top and bottom improved the stability of the sample during the setting up of the test.

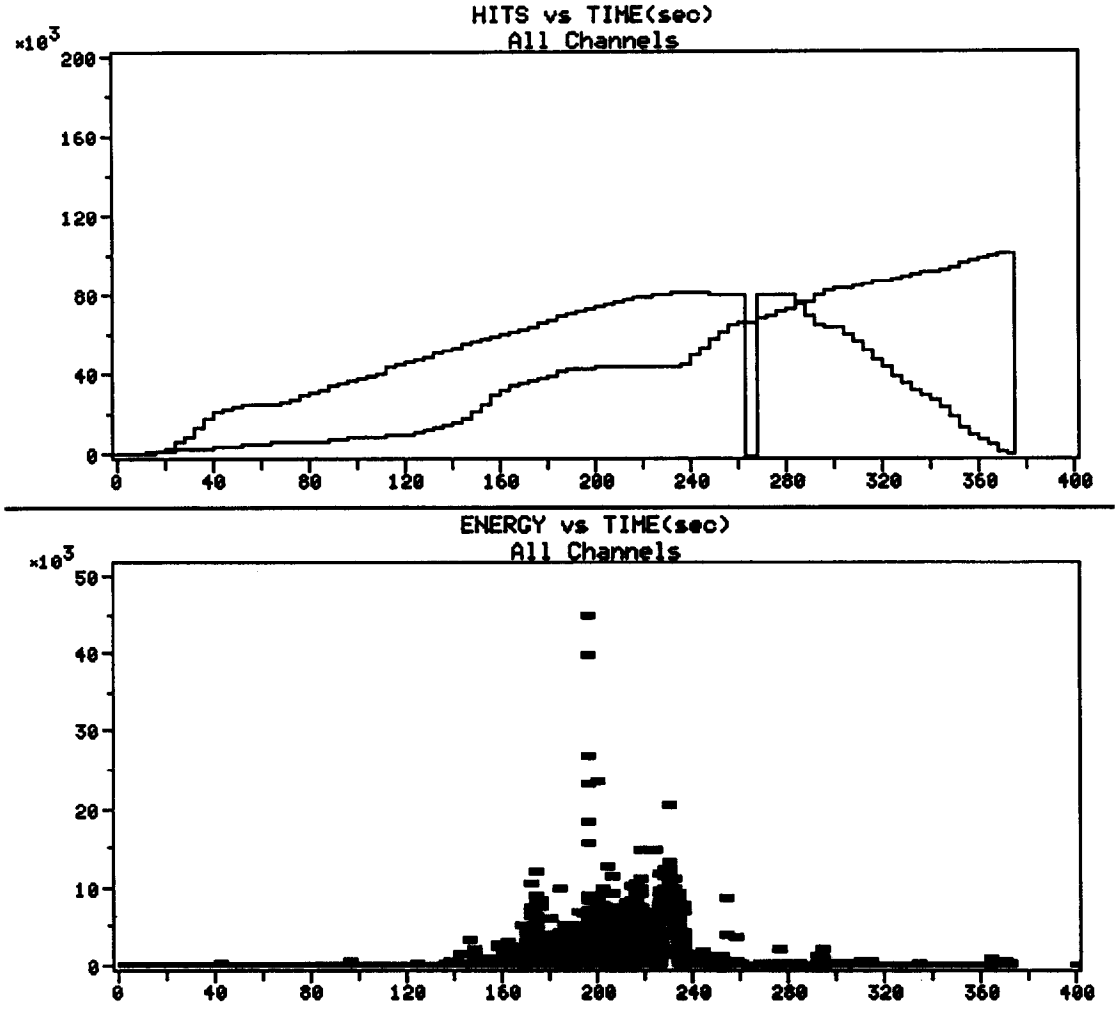


*Figure 2. Acoustic emission characteristics for sample of Elsburg Quartzite loaded to 200 MPa. A: load and number of acoustic emissions with time. B: acoustic energy release rate with time.*

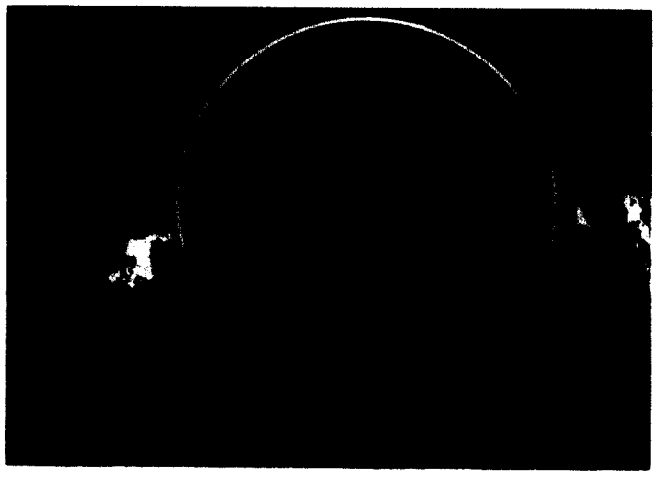

*Figure 3. Detail of test of Elsburg quartzite block to 258 MPa vertical stress at a k-ratio of 0.5, showing the spalling. The white circle represents the approximate position of the original hole (25-mm diameter).*

*Figure 4. Detail on test of layered block with applied pressure of 200 MPa and a k-ratio of 0.5.*

### 2.2 Results

The Norite samples were loaded at a k-ratio of 0.3 and exhibited the classical failure pattern of primary cracking followed by remote crack formation and spalling. The higher k-ratio of 0.5 applied in the Elsburg tests prevented the formation of the primary cracks in most cases. Spalling initiated at the tunnel sidewalls when the vertical stress was about 1.1 times the unconfined compression strength

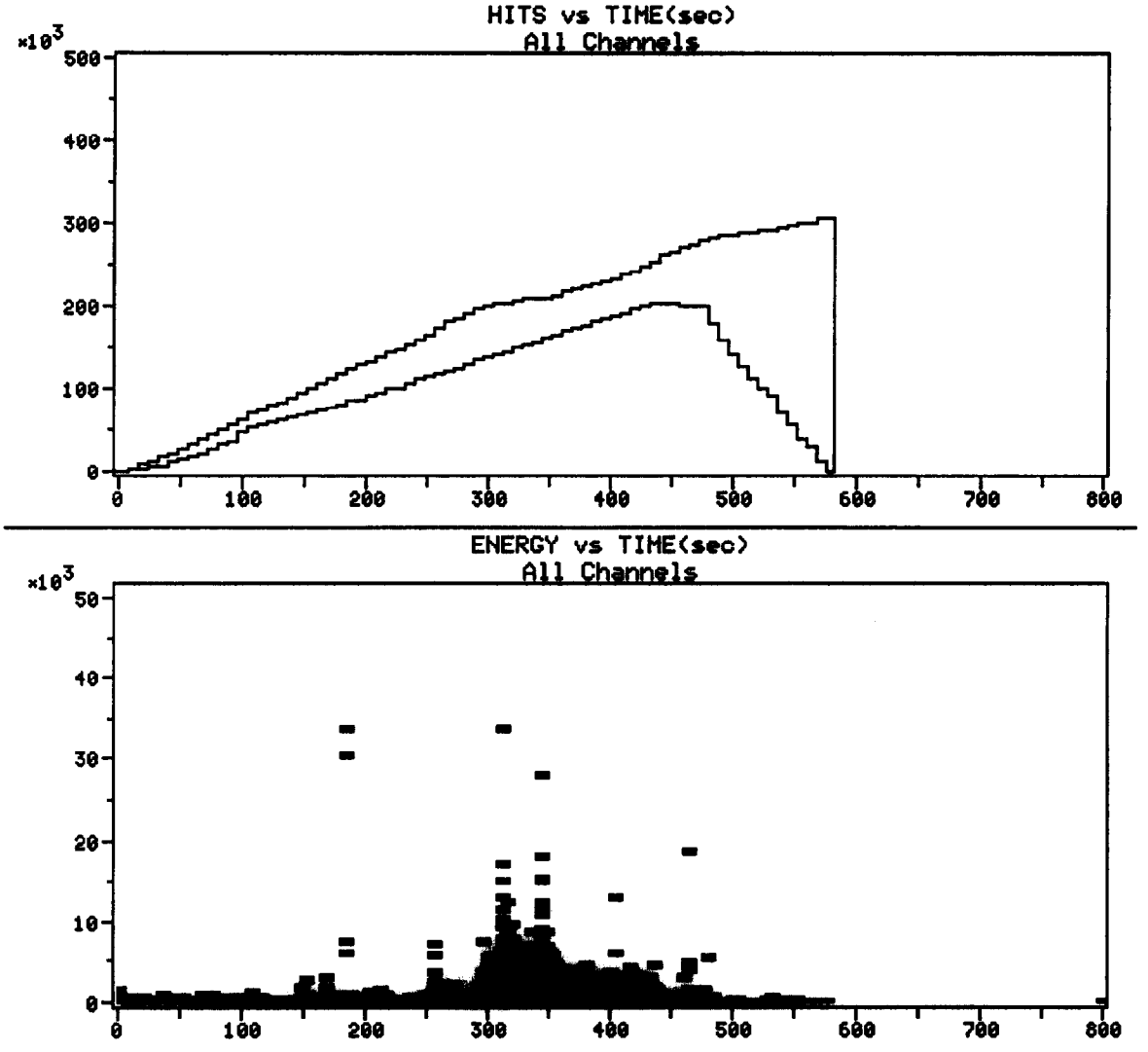


*Figure 5. Acoustic emission events for the layered block loaded to 200 MPa. A: AE and load versus time. B: energy release rate versus time.*

(UCS). At a vertical applied stress of about 1.6 times the UCS, the confinement was felt to drop. After this stage, the pump providing confinement had to be continuously pumped in order to maintain a particular pressure. The acoustic emission energy release is shown in Figure 2.

Increasing the applied vertical pressure and the lateral confinement at the same k-ratio led to continued spalling from the sidewalls, as shown in Figure 3. The AE initiates at about 125 MPa (63 percent of the maximum load) and the main energy release occurs at 175 MPa (1.5*UCS). The sample could no longer sustain load once the vertical stress reached twice the UCS. At this stage, the spalling extended a distance of 5 mm outside the original radius, as shown in Figure 3. The characteristic sharpening of the hole is observed. The large increase of low-energy AE during the constant load period must be linked to time-dependent fracture processes associated with the spalling. Some AE activity is evident during unloading and would be due to fracturing caused by the relief of residual stresses.

A detail of the fracture pattern around the hole in the layered block is shown in Figure 4. The core was not removed from the central rock layers so as not to damage the plates. Even though they are horizontal, the discontinuities appear to have had a significant effect on the fracture pattern. On the right-hand side, the spalling has resulted in a triangular region of breakout that does not seem to be affected by the presence of the joint. Sidewall parallel fractures extend some distance into the rock, much further than the corresponding solid block. Most of the fracturing is confined to the two central layers,

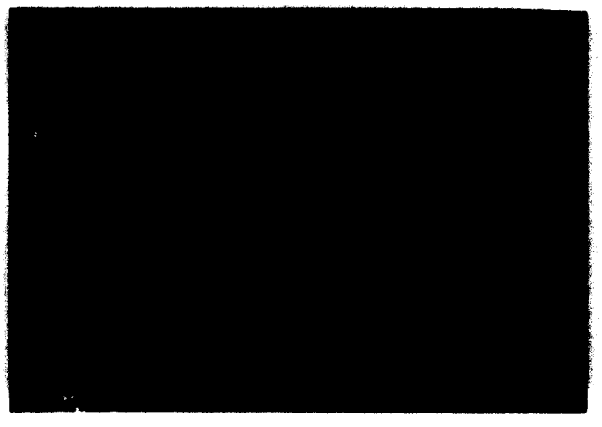

*Figure 6. Fracturing of the rock in the central layer of the layered block with applied pressure of 200 MPa and a k-ratio of 0.5 .*

as has been observed underground with inclined layers (Goodman 1972; Roberts et al. 1999).

The acoustic emission release pattern, as shown in Figure 5, is different from that of the solid block, and the increase in the number of events is proportional to the loading. The total number of events is about three times that observed in the solid block. This increase in AE can be ascribed to the production of additional fracturing due to the presence of the discontinuities. The first set of higher energy releases when the vertical loading is about 60 MPa (30 per cent of maximum load). The largest events occur around 100 MPa, and the event size appears to reduce after 150 MPa. Fewer AE events are evident during the constant load stage and the unloading.

The change in the fracturing along the length of the hole can been seen on the surface of the layers, as shown in Figure 6. The sidewall fractures initiate at about 1 borehole diameter from the face and extend outwards along the axis of the hole. The fracturing is less advanced in the layer above. Fracturing within the longer core stub of Figure 6 is indicative of the petal-centre line mode of failure observed in core from boreholes (Li and Schmitt 1998). Alternatively, the fracture suggests that the core was loaded between the platen and the rock and experienced stress conditions similar to those of an unconfined compression test.

## 3. Numerical Modelling

### *3.1 Model for fracturing in compression*

The mechanism of initiation of the slabbing fractures parallel to the major principal compressive stress, in a compressive stress state, has been a topic of considerable discussion. Initiation of fractures parallel to the sidewall is not consistent with elastic materials and has to be due to microscopic inhomogeneities within the rock (Ewy and Cook 1990a). The sliding flaw mechanism has been extensively applied to study splitting in uniaxial tests, but was shown to have a limited ability to cause sidewall slabbing, except at very close distances from the hole (Ewy and Cook 1990a). Analytical (Ewy and Cook 1990b) and numerical models (Zheng 1989) based on linear elastic fracture mechanics predict the formation of infinitely many parallel slabs in the breakout zone.

The term *compression fracture* is thus a misnomer, as fracture is associated with extensional deformation (Stacey 1981). It is the mechanism through which extensional deformation occurs that differs between compressive and tensile fields. There is no single mechanism governing the evolution of inelastic deformation in heterogeneous, quasi-brittle materials subject to compressive stress fields. The physical manifestation is realised through myriad micromechanical processes, including differences in compliances of constituent material grains and the interaction between different crack, pore and grain configurations.

The inability to consider all possible micromechanical mechanisms and their spatial distribution dictates the adoption of a phenomenological model. This model must exhibit the global system response resulting from the micromechanical interactions and yield extensional inelastic deformation orthogonal to the direction of applied compression. It is this inelastic extensional strain that governs the discrete fracture criteria.

The Mohr-Coulomb criteria is a frictional dissipative mechanism independent of the intermediate principal stress and is a suitable phenomenological description of compressive failure in quasi-brittle materials. It is a linear approximation of the Mohr envelope and provides a conservative strength limit, especially at low confinements. The Mohr-Coulomb yield criteria is given by

$$\sigma_1 - \sigma_3 + (\sigma_1 + \sigma_3)\sin\varphi = 2C\cos\varphi \qquad (1)$$

where C and $\varphi$ are the cohesion and friction angle, respectively, both functions of an effective plastic strain measure

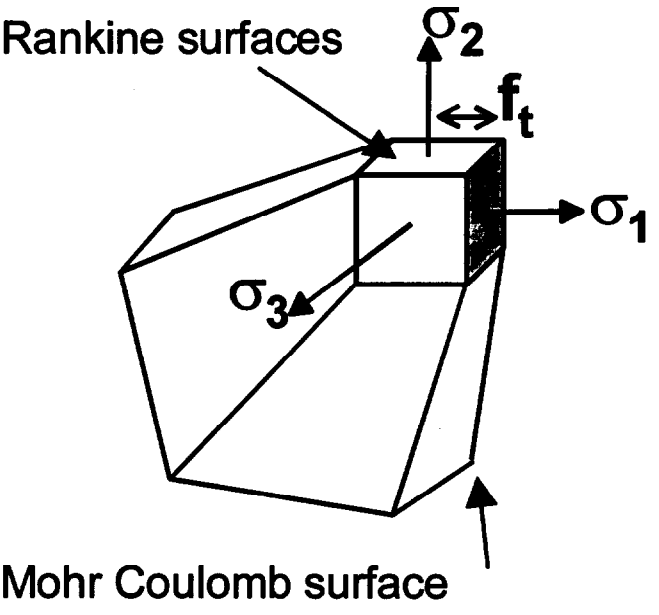


*Figure 7. Schematic of yield surfaces in three-dimensional Mohr-Coulomb-based fracture model.*

$\varepsilon^p = \sqrt{\varepsilon_i^p}\,\varepsilon_i^p$. The non-associative form of the Mohr-Coulomb criteria is adopted with the plastic potential function given by Equation 1 with the friction angle (replaced by a dilation angle $\psi$ (also a function of the effective plastic strain measure $\varepsilon^p$).

The standard form of the Mohr-Coulomb criteria provides a poor description of the tensile behaviour of quasi-brittle materials. To improve the tensile description, a three-dimensional rotating crack (smeared crack) model is coupled with the Mohr-Coulomb yield surface. This introduces a triad of intersecting, orthogonal tensile planes in the tensile region of the yield surface, as shown in Figure 7. The yield function for each tensile plane is given by

$$\sigma_i - f_t + h\,\varepsilon_i^p = 0 \qquad i = 1, 2, 3 \qquad (2)$$

where $f_t$ is the tensile strength, $\varepsilon_i^p$ is the inelastic strain component in the $i$-th principal stress direction and $h$ is the plastic softening modulus which is normalised by the fracture energy to ensure discretisation-independent energy dissipation.

The inelastic extension strain realised through compressive yield is coupled with the tensile strength degradation in Equation (2) such that compressive yield induces tensile yield in the orthogonal direction. The proposed model correctly exhibits the physical manifestation, yielding cracks that develop sub-parallel to the opening. These cracks are able to link up with increased loading to form discontinuities on which frictional slip may be realised. The process is wholly extensional, with the phenomenological shear criteria simply a convenient means of relating compressive deformation to orthogonal extensional deformation.

There is a scale effect in borehole breakout problems (Martin 1997; Gay 1973; Goodman 1972), and the failure stress is found to reduce with increasing hole diameter and appears to remain approximately constant above a characteristic dimension. A further drop in strength was observed when considering underground tests. The Mohr-Coulomb model is a stress based criteria and therefore exhibits no size effect. Size effect may be introduced through a non-local implementation or possibly through the normalisation of the cohesion degradation by an energy term in the spirit of the crack band model.

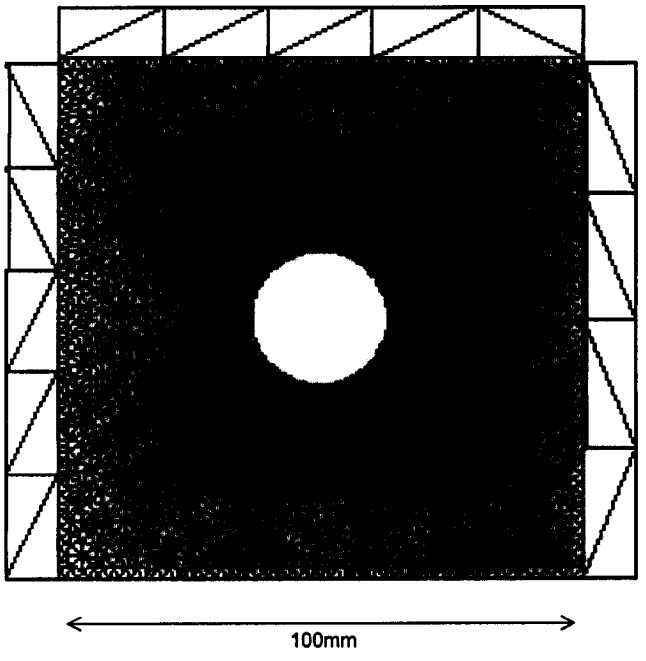


*Figure 8. Finite element mesh of laboratory model.*

### 3.2 Modelling of experiments

The material model has been implemented in the finite/discrete element code ELFEN. Models of the two blocks were created with a mesh of constant strain triangles, as shown in Figure 8. The mesh was refined near the hole, with an element size of 0.5 mm. Previous experience has shown that when modelling laboratory tests, it is important to represent the boundary conditions correctly (Sellers and Scheele 1996). Therefore, stresses were applied to the outer sides of the steel platens confining the sample. The left side of the left platen was fixed in the horizontal direction and the bottom was fixed in the vertical direction. The friction angle between the platen and sample is set to 5 degrees and the friction angle between the rock layers is 30 degrees.

The fracture patterns for the solid and layered block are shown in Figure 9a and Figure 9b, respectively. The patterns clearly demonstrate that the model is able to represent the difference in fracture patterns. In the solid block, there is no primary fracturing, and the spalling is represented by fractures forming sub-parallel to the hole. Bending of the rock layers alters the fracture pattern from the solid block, causing an extended fracture zone that remains confined within the central plates. This is exactly as observed in the laboratory tests.

The numerical equivalent measure of the acoustic emission is the kinetic energy release (Napier 1991). The kinetic energy is plotted with time for the two samples in Figure 10 and in both cases is similar to the observed acoustic emission data. The pattern of energy release for the solid block shows a sudden increase at about 180 MPa, close to the value of applied stress observed in the acoustic emission data. Kinetic energy release occurs at a lower stress level of around 150 MPa in the layered block, and continues over a wider range of applied stress than in the solid block.

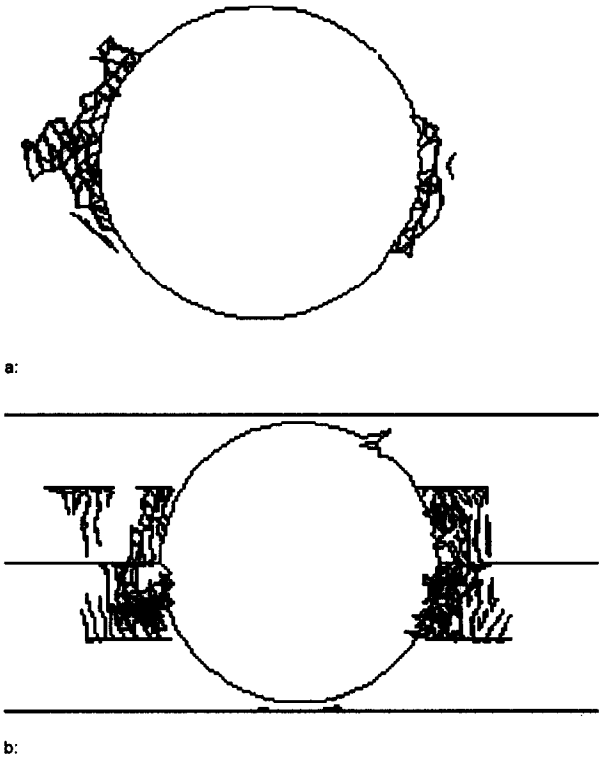


*Figure 9. Fracture pattern in models at a vertical applied stress of 200 MPa and 100 MPa horizontal stress for a: the solid block and b: the jointed block.*

## 4. Conclusions

Physical model tests have confirmed that discontinuities in the rock mass can alter the fracture patterns associated with an excavation. The discontinuities induce more fracturing than is observed in the solid blocks. Thus, the extent of fracturing expected in deep level mining excavations will be greater than predicted from borehole breakout analyses. The numerical model that has been developed is able to predict the change in fracture pattern and the increase in fracture extent due to the discontinuities and the load level at which failure can be expected. At present, the model parameters must be adjusted for the scale effect to predict the underground strength; however the model can be easily extended to a non-local, energy based formulation to include the scale effect explicitly.

The finite/discrete element numerical model with compression fracturing is well suited for modelling the fracture formation in deep tunnels and for gaining an understanding of the interaction between the changing loading conditions, the support and dynamic loading due to seismic events.

## 5. Acknowlegements

Experimental work was performed as part of Deep Mine projects 7.1.1, 8.2.1 and 12.3.3. The numerical modelling forms part of projects STEP Y1742 and Y1950. Funding is gratefully acknowledged. Thanks are extended to Drs J. Kuijpers, J.A.L. Napier, D.F. Malan, D. Roberts, and T.R. Stacey for helpful discussions.

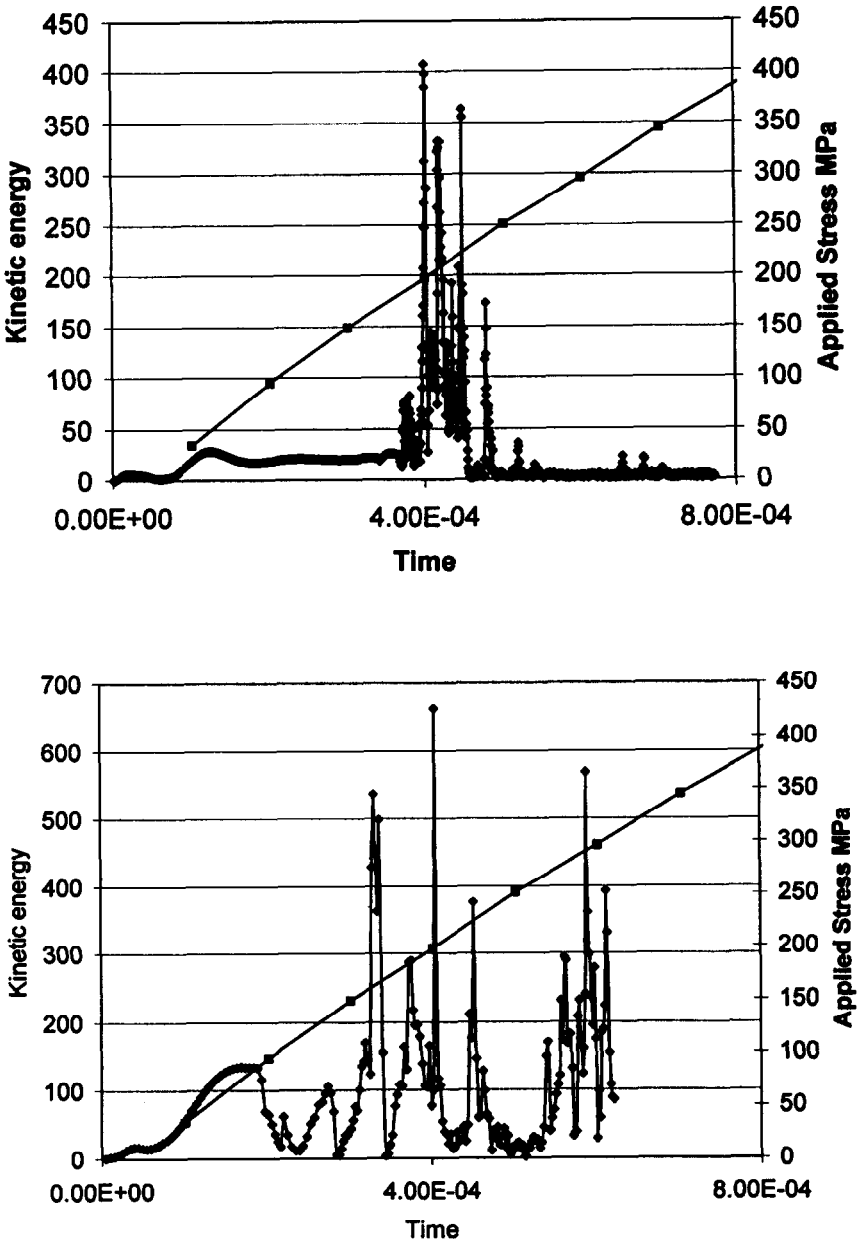


*Figure 10. Kinetic energy change with time for a: solid block and b: layered block.*

## 6. References


Barla, G. 1972. The distribution of stress around a single underground opening in a layered medium under gravity loading. *Int J. Rock Mech. Min Sci.* **9**, 127-154.

Bosman J.D., Malan, D.F., and Drescher, K. Time dependent deformation at Hartebeestfontein Mine. *Tunnels under Pressure: AITES / ITA World Tunnel Congress 2000,* 55-62. Johannesburg: The South African Institute of Mining and Metallurgy.

Brady, B.H.G. and Brown, E.T. 1993. *Rock Mechanics for Underground Mining.* London: Chapman and Hall.

Carter, B.J. 1992. Size and stress gradient effects on fracture around cavities. *Rock Mech. Rock Engng,* 167-186.

Carter, B.J., Lajtai, E.Z., and Petukhov, A. 1991. Primary and remote fractures around underground cavities. *Int J. Num Anal. Meth. Geomechanics* **15**, 21-40.

Chen, S-H. and Egger, P. Three-dimensional elasto-viscoplastic finite element analysis of reinforced rock masses and its application. *Int. J. Numer. Anal. Meth. Geomech* **23**, 61-78.

CSIR. 1973. An investigation of factors influencing the behaviour of models of underground excavations. CSIR internal report ME / 1173/7 April 1973.

Ewy, R.T. and Cook, N.G.W. 1990a. Deformation and fracture around cylindrical openings in rock—I: observation and analysis of deformations. *Int J. Rock Mech. Min Sci.* **27**, 387-407.

Ewy, R.T. and Cook, N.G.W. 1990b. Deformation and fracture around cylindrical openings in rock ñ II initiation, growth and interaction of fractures. *Int. J. Rock Mech. Min Sci.* **27**, 409-427.

Gay, N.C. 1973. Fracture growth around openings in thick-walled cylinders of rock subjected to hydrostatic compression. *Int. J. Rock Mech. Min Sci.* **10**, 209-233.

Goodman R., Heuze, F.E., Bureau, G.J. 1972. On modelling techniques for the study of tunnels in jointed rock. *Rock Mechanics* 441-479.

Graham P.C. Some problems associated with the use of a tunnel machine in deep-level gold mines.

Haimson, B. and Song, I. 1998. Mechanics of rock fracturing around boreholes. *Mechanics of Jointed and Faulted Rock* (H.P. Rossmanith, ed): *Proceedings of the Third International conference on jointed and faulted rock. MJFR-3. Vienna 1998,* 325-330.

Kulhawy, F. 1975. Stresses and displacements around openings in rocks containing an elastic discontinuity. *Int J. Rock Mech. Min Sci.* **12**, 59-72.

Li, Y. and Schmitt, D.C. 1998. Drilling induced core fractures and in situ stress. *J. Geophys Res* vol **103** (B3), 5225-5239.

Malan, D.F. and Basson, F. 1998. Ultra-deep mining: The increased potential for squeezing conditions. *J. S. Afr. Inst. Min. Metall.*, 353-363.

Martin, C.D. 1997. Seventeenth Canadian Geotechnical colloquium: the effect of cohesion loss and stress path on brittle rock strength. *Can. Geotch. J. Vol* **34**, 698-725.

Napier, J.A.L. 1991. Energy changes in a rockmass containing multiple discontinuities. *Jour. S. Afr. Inst. Min. Metall.* 91(5), 145-157.

Rech, J.M., Otto, W.M. and Hagan, T.O. 1992. Attempts to combat scaling and blockage problems in deep mine ore passes. *Proc. Symp. on Orepasses and combustible materials underground. Association of Mine Managers of South Africa,* 221-240.

Roberts, D.P., Sellers, E.J. and Sevume, C. 1999. Numerical modelling of fracture zone development and support interaction for a deep level tunnel in a stratified rockmass. *SARES 99. SANIRE, 1999, Johannesburg.*

Sellers, E. and Scheele, F. 1996. Prediction of anisotropic damage in experiments simulating mining excavations in Witwatersrand Quartzite blocks. *Int J. Rock Mech Min Sci* **33** (7), 659-670.

Stacey, T.R. 1981. A simple extension strain criterion for fracture of brittle rock. *Int. J. Rock Mech. Min Sci.* **18**, 469-474.

Swoboda, G., Yang, Q., and Shen, X.P. 1998. An energy based damage model of jointed rockmass. Mechanics of Jointed and Faulted Rock. Rossmanith H. P. (ed). *Proceedings of the Third International Conference on Jointed and Faulted Rock. MJFR-3, Vienna 1998,* 291-298.

Zheng, Z., Kemeny, J. and Cook, N.G.W. 1989. Analysis of borehole breakouts. *J. Geophys Res.* **94**, 7171-7182.